# SILICON QUANTUM DOT ABSORBER LAYERS FOR ALL-SILICON TANDEM SOLAR CELLS: OPTICAL AND ELECTRICAL CHARACTERISATION

P. Löper[†‡], A. Hartel[†], M. Künle[†], D. Hiller[‡], S. Janz[†], M. Hermle[†], M. Zacharias[‡], S. W. Glunz[†]
[†]Fraunhofer Institute for Solar Energy Systems, Heidenhofstr. 2, D-79110 Freiburg, Germany
[‡] IMTEK, Georges-Koehler-Allee 103, D-79110, Germany
Corresponding author: Philipp Löper, Phone: +49 761 4588 5475, Fax: + 49 761 4588 9250
philipp.loeper@ise.fraunhofer.de

ABSTRACT: Silicon carbide thin films that incorporate silicon nanocrystals are investigated. The optical band gap of the films is controlled by the deposition and annealing conditions. The band gap of as-deposited films was varied between 2.1 eV and 3 eV. $Si_{0.5}C_{0.5}$ films were successfully doped in-situ with $B_2H_6$ and conductivities of $5 \cdot 10^{-5}$ S/cm to $2 \cdot 10^{-4}$ S/cm were obtained. Temperature dependent conductivity shows that the conductivity follows an Arrhenius relation for certain temperature regimes. However, the temperature dependence over a larger temperature range is not Arrhenius-like, which is in agreement with previous results.
Keywords: all-Silicon Tandem Solar Cell, Silicon Nanocrystals

## 1 INTRODUCTION

The radiative efficiency of bulk silicon (Si) solar cells under the AM1.5G spectrum is limited theoretically to 29% due to the incomplete utilization of high energy photons and transmission of photons with less energy than the Si band gap. One way to enhance the efficiency is to use a stack of solar cells, in which each cell has a band gap that is optimized for the absorption of a certain spectral region. The theoretical efficiency of tandem solar cells with a bulk Si bottom cell increases to 42.5 % when one additional solar cell with 1.8 eV band gap is used and to 47.5 % with two further solar cells with band gaps of 1.5 and 2 eV placed on top of the bulk Si cell [1]. Promising materials for the fabrication of silicon based high band gap solar cells are silicon quantum dots in dielectrics. The charge carrier confinement in Si quantum dots leads to a higher band gap of the compound material and is a function of the quantum dots dimensions. Controlling the silicon nanocrystal (Si NC) size therefore enables the adjustment of the band gap. This makes it possible to fabricate silicon based top and middle cells that may be used as building blocks in all-silicon tandem solar cells (see figure 1). The possibility to fabricate Si NC by plasma enhanced chemical vapour deposition (PECVD) or sputtering techniques allows for the cost efficient deposition of the top and/or middle solar cell. This suggests two application strategies for Si NC solar cells: The high band gap Si NC may be deposited onto a high-efficiency wafer-based Si cell in order to target highest conversion efficiencies. Furthermore, the Si NC solar cell could also serve in a superstrate configuration for the deposition of a c-Si thin film solar cell in a low cost approach.

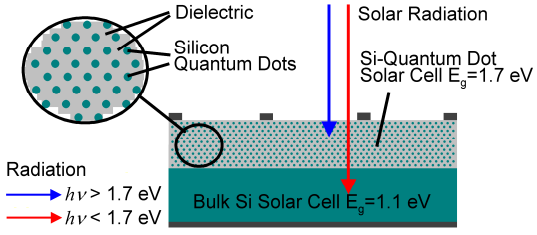


**Figure 1:** Principle of an all-silicon tandem cell with a quantum dot top solar cell (left). The control of the band gap allows extending the concept to multi solar cells employing three or more cells. The band gap is tuned by a size control of the Si nanocrystals employing a multilayer approach [6].

Silicon quantum well and dot structures for solar cells have been reported by several authors [2, 3] in recent years. Significant effort has been made concerning the controlled fabrication of silicon nanocrystals and also first devices could be realized [2, 4].

However, the open circuit voltage of Si NC solar cells on insulating substrates could not yet be improved above 400 mV [5]. In order to proof charge carrier confinement electrically, the open circuit voltage has to be at least higher than for bulk Si solar cells, e.g. at least >700 mV. Compared to this value, 400mV is still low. In order to realize a higher open circuit voltage, the conduction mechanism through the nanocrystal network and recombination in the absorber layer and at the interfaces has to be further investigated.

This paper consists of two parts: In the first part, $Si_xC_{1-x}$ layers with compositions between x=0.2 and x=0.8 are characterized by UV-Vis and photoluminescence spectroscopy. In previous experiments [7] we analyzed the structural transformation of the $Si_xC_{1-x}$ layers due to annealing steps at different temperatures. It was shown how Si NC evolve in the silicon rich SiC layers and how at higher temperatures also SiC NC are formed. The next step towards a solar cell with an absorber layer made of Si NC in a SiC matrix is doping of the SiC layer. Doping of nanostructures imposes many question, and is intensively being investigated currently [8-10]. For example, recent experiments on Si NC obtained by a pyrolysis synthesis show that phosphorus donor states and Si dangling bonds contribute to dark conductivity, but act as recombination centers under illumination [11]. Only few studies on


**Figure 2:** Schematic of size control for silicon in a Si based dielectric matrix. Layers with silicon excess are deposited alternatingly between stoichiometric layers. The stoichiometric layers act as a diffusion barrier for the silicon atoms and therefore limit the growth of silicon nanocrystals during the annealing step.

charge separation in Si NC networks have been carried out [12], and especially the contributions of Si NCs and their surrounding dielectric matrix to transport and recombination is still not known. Therefore, we present first experiments on doping the $Si_{0.5}C_{0.5}$ matrix in the second part of this paper. Doping was done in-situ with $PH_3$ and $B_2H_6$ as precursor gases. The electrical properties are analyzed by dark DC conductivity and temperature dependent conductivity measurements.

## 2 EXPERIMENTAL

Amorphous silicon carbide layers were deposited in a lab type AK400 PECVD reactor from Roth&Rau. The reactor features two plasma sources that operate at 13.56 MHz (HF) and 2.45 GHz (MW). Silane ($SiH_4$), methane ($CH_4$) and argon (Ar) were used as precursor gases.

Two sample series are investigated in this paper: One series with varying $SiH_4$ and $CH_4$ gas flows to control the composition of the a-$Si_xC_{1-x}$:H layer. For this series, the deposition parameters were set to p=0.05 mbar, T=250 °C, 2·300 W MW power, 5 W HF power, and 140 sccm argon. $SiH_4$ and $CH_4$ flows were varied between 5 sccm and 20 sccm, but the total $SiH_4$+$CH_4$ flow was kept constant, see table I. The composition was determined by Rutherford backscattering and Auger Electron Spectroscopy (AES). The samples were deposited on different types of substrates. Quartz substrates (Heraeus "Suprasil 300") were used for the reflectance- and transmittance measurements. For the PL measurements we used (111)-oriented CZ-Si. This sample series was used for optical characterization of $Si_xC_{1-x}$ layers. The structural transformation of this series are reported in [7].

After deposition a subsequent thermal annealing step was performed. The optical properties of the amorphous layers were analysed by UV-Vis and photoluminescence (PL) spectroscopy. Annealed layers with the composition $Si_{0.8}C_{0.2}$ were investigated by PL spectroscopy.

For PL measurements, the 514.5 nm line of an argon ion laser was used and the luminescence was detected with an Andor shamrock 303i spectrograph and an Andor iDUS DU401A-BRDD CCD camera. The spectrograph had 303 mm focal length, an aperture of f/4 and a 300 l/mm grating. The relative transmission function of the detection system was determined using a reference lamp with known spectrum and all spectra were corrected for the relative transmission.

**Table I:** Gas flows used for the deposition of the $Si_xC_{1-x}$ layers. These layers were used to study the optical properties of SiC layers with varying stoichiometry under annealing. The composition was determined by Rutherford Backscattering Spectrometry (RBS) and Auger Electron Spectroscopy (AES).

| Composition of $Si_xC_{1-x}$ | $SiH_4$ (sccm) | $CH_4$ (sccm) | Ar (sccm) |
|---|---|---|---|
| x=0.80 | 20 | 5 | 140 |
| x=0.65 | 15 | 10 | 140 |
| x=0.55 | 12 | 12 | 140 |
| x=0.45 | 10 | 15 | 140 |
| x=0.20 | 5 | 20 | 140 |

UV-Vis spectroscopy was performed with a Varian Cary 500i photospectrometer using an integrating sphere to measure reflectance ($R$) and transmission ($T$) spectra. The absorption coefficient $\alpha$ was calculated as $\alpha = 1/d \cdot \ln((1-R)/T)$. The thickness $d$ was determined from transmission and ellipsometry measurements and cross-sectional Scanning Electron Microscope (SEM). The optical band gap was determined with Tauc's method [13] which relates the optical band gap $E_{g,Tauc}$ to the absorption coefficient $\alpha$ as $\alpha\hbar\omega = A(\hbar\omega - E_{g,Tauc})^2$. $A$ is a constant and $\hbar\omega$ the photon energy. Because the Tauc method is only an approximate relation, we compare it also to the $E_{04}$ optical gap and the position of the PL maximum. $E_{04}$ is the photon energy at which the absorption amounts $10^4$ 1/cm [14].

Doping experiments were performed with stoichiometric SiC layers (composition $Si_{0.5}C_{0.5}$) that would later be used as the intermediate diffusion barrier layer as depicted in figure 2. The following deposition parameters were chosen: p=0.05 mbar, T=350 °C, 2·1000 W MW power, 150 W HF power, 30 sccm Argon, $SiH_4$=40 sccm and $CH_4$=60 sccm. The layers were doped in-situ using $B_2H_6$ or $PH_3$ as precursor gases with flows of 3 sccm, 10 sccm, 20 sccm, 30 sccm and 40 sccm. The resulting film composition $Si_{0.5}C_{0.5}$ was monitored by Rutherford backscattering, secondary ion mass spectroscopy and auger electron spectroscopy.

Dark DC conductivity measurements were taken for electrical characterization. The sheet resistance was measured at room temperature to evaluate the effect of dopants. Temperature dependent dark conductivity experiments were performed to investigate electrical transport more in detail. For these electrical measurements, a HP 4140B Ampèremeter was used to apply a voltage $V$ to the sample and to measure the current $I$ through the sample. Measurements were performed under vacuum in a cryostat at temperatures between 77 K and 400 K. Dark conductivity measurements were performed on samples with coplanar evaporated Aluminium electrodes with 3 mm spacing between adjacent electrodes. The total resistance $R_{total}=U/I$ is the sum of the thin film resistance $R_{TF}$ and the resistance of the contacts $R_C$. The resistance of the thin film between two electrodes of distance $D$ and width $L$ is $R_{TF}=(R_{sh}D)/L$, yielding $R_{total}=R_C+R_{SH}\cdot D/L$. A linear fit to the data ($R_{total}$, $D$) provides the sheet resistance of the film under consideration [15]. In order to evaluated the sheet resistance, $I(V)$ curves were measured for different distances $D$ between two electrodes using also electrodes that were not direct neighbors, e.g. with one intermediate electrode in between. This non-optimized electrode geometry allows for an estimate of the sheet resistance, but not for an evaluation of the contact resistances and will be replaced by a more advanced structure shortly.

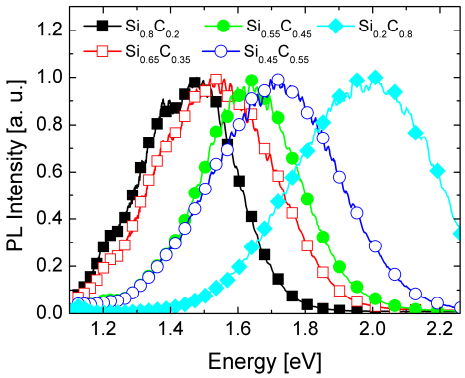


**Figure 3:** Photoluminescence (PL) spectra of $Si_xC_{1-x}$ samples. The PL peak shifts to higher energies with more carbon content and also becomes broader. The broader peak shape can be explained by wider band tails in the carbon rich samples.

## 3 OPTICAL PROPERTIES

Figure 3 depicts normalized PL spectra of a series of as-deposited a-$Si_xC_{1-x}$:H samples with varying composition x. A shift of the PL peak to higher photon energy can be observed when the carbon content in the $Si_xC_{1-x}$ is increased. The peak shift is explained by the higher band gap [14] due to incorporation of carbon into the amorphous network. In addition, the blueshift is accompanied by a broader peak shape. This is commonly explained by wider band tails that are induced by the increased disorder resulting from higher carbon incorporation into the amorphous lattice and is in good agreement with previous PL studies of amorphous silicon carbide [14, 16].

The maximum of the PL peak is one measure to characterize the optical band gap of amorphous materials. Other measures are deduced from absorption measurements employing the Tauc analysis or evaluating $E_{04}$ as described above. Figure 4 shows the value of the band gap as obtained from these three methods for a samples series with varying composition. The values of $E_{04}$ and $E_{g,Tauc}$ are in good agreement with each other and show that the band gap increases linearly with the carbon

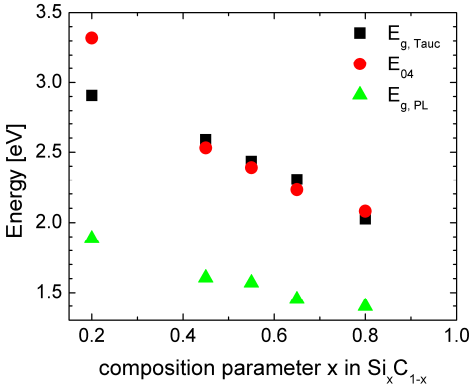


**Figure 4:** Optical gap of the as-deposited samples as a function of the composition of the samples. The optical gap was determined by an evaluation of the optical gap after Tauc, $E_{04}$ and the PL peak.

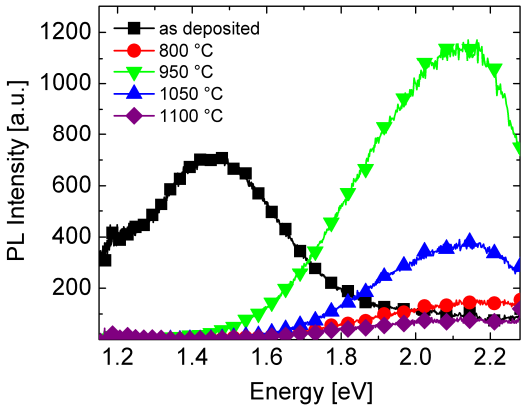


**Figure 5:** PL of the $Si_{0.8}C_{0.2}$ sample after annealing for 30 min at different temperatures. Within the series of increasing annealing temperatures, the PL signal reaches a pronounced maximum at 950 °C annealing and decreases again for even higher annealing temperatures.

content of the as-deposited a-$Si_xC_{1-x}$:H samples. The optical gap deduced from the PL peak energy is lower than $E_{04}$ and $E_{g,Tauc}$. This effect can be explained by the fact that charge carriers first thermalize into localized states and then recombine, while the Tauc analysis evaluates transitions from extended to extended states. The increase with carbon content of the PL peak energy is also linear, but not as steep compared to $E_{04}$ and $E_{g,Tauc}$. The increasing difference is attributed to widened band tails due to carbon incorporation and was described by Siebert [14] in detail.

Figure 5 shows the PL from the sample $Si_{0.8}C_{0.2}$ after annealing under 1050 mbar $N_2$ for 30 min at different temperatures. A blueshift of the PL peak due to annealing is observed. In this experiments, temperatures of 800 °C, 950 °C, 1050 °C and 1100 °C were chosen. The position of the PL maximum is ~2.15 eV and does not depend on the annealing temperature. Thus, the band gap as determined by the PL peak energy is ~0.7eV higher than for the non-annealed sample. However, the PL intensity is strongly reduced for all annealing temperatures apart from the 950°C anneal. Within the series of increasing annealing temperatures, the PL signal reaches a pronounced maximum at 950 °C annealing and decreases again for even higher annealing temperatures. In [7] it was demonstrated that Si NC begin to crystallize around 700°C and reach their maximum size after ~900°C annealing. At temperatures between 1000°C and 1100°C, SiC NC begin to form. Therefore, we attribute the PL of the sample annealed at 950°C to Si NC and conclude that the formation of SiC nanocrystals quenches the PL. However, the origin of the PL –whether is stems from the Si NC volume or the interface between the Si NC or the surrounding SiC matrix- still has to be clarified.

## 4 ELECTRICAL PROPERTIES

The electrical properties of stoichiometric $Si_{0.5}C_{0.5}$ layers were investigated to assess their potential to serve as a conductive intermediate layer between two layers with Si NC (see figure 2). Due to technological restrictions, these layers were annealed at only 800°C.

### 4.1 Dark conductivity

Figure 6 shows the conductivity of $Si_xC_{1-x}$ samples

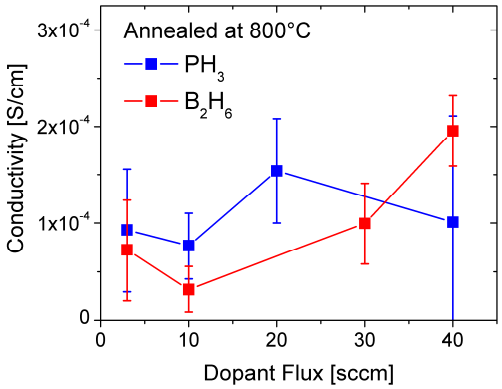


**Figure 6:** Sheet resistance of doped SiC thin films. Phosphine (PH3) and Diborane (B2H6) were used as in-situ doping gases. After deposition, the samples were annealed at 800°C.

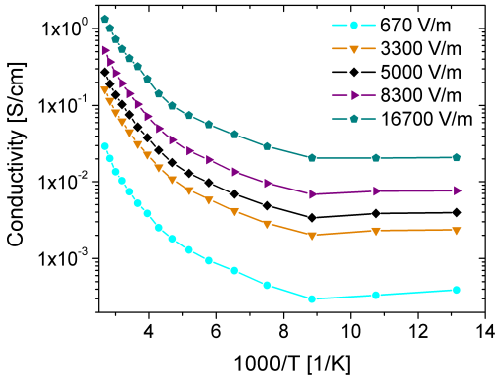


**Figure 7**: Temperature dependence of the conductivity of a SiC layer. At high temperatures, 250 K<T<400 K, the conductivity obeys roughly an Arrhenius law. For lower temperatures, however, the slope of the Arrhenius plot changes. Similar dependences were previously found by Anderson and Spear [19] and Bullot [20].

that were in-situ doped with $PH_3$ or $B_2H_6$ and annealed at 800°C. The conductivity was calculated by dividing the sheet resistance by the film thickness (80nm). The value of the conductivity is comparable to unannealed amorphous silicon carbide layers [17, 18]. An increase of the conductivity due to boron doping of the samples can be seen. However, no clear trend is observable for phosphorus doping. This might be due to the aluminum contacts used for this experiment. Aluminum does not form good contacts with phosphorus doped a-SiC, and mostly nickel is used instead. However, nickel metallization was not yet accessible.

### 4.2 Temperature activated conductivity

For a more detailed investigation of the electrical properties we performed conductivity measurements as a function of the sample temperature. After annealing at 800 °C, only small crystalline domains are expected, but most of the film is still amorphous. Electrical transport through amorphous solids takes place by different mechanisms. The localized states of the band tails act as traps and transport takes place by thermally activated hopping of charge carriers. The conductivity of the tail states $\sigma_{tail}$ is described by $\sigma_{tail}=\sigma_{0,tail}\cdot exp(-(E_{CT}-E_F)/kT)$. $E_{CT}$ is the activation energy for this process, $E_F$ the Fermi energy, $k$ the Boltzmann constant and $T$ the temperature. $\sigma_{0,tail}$ is a prefactor. The activation energy for transport through the extended states in the conduction (or valence) band is the difference $E_C$-$E_F$ of the band edge $E_C$ and the Fermi level $E_F$. Thus, the conductivity reads $\sigma_{ext}=\sigma_{0,ext}exp(-(E_C-EF)/kT)$. While amorphous Silicon follows very well the expected Arrhenius law, the temperature dependence of SiC films is different and not yet explained. Figure 6 depicts the temperature dependence of the conductivity for a series of different applied voltages. Several regimes of the temperature dependence can be identified. At high temperatures, 250 K<$T$<400 K, the conductivity obeys roughly an Arrhenius law, e. g. $\sigma \sim exp(-const/T)$. Similar dependences were previously found by Anderson and Spear [19] and Bullot [20]. For lower temperatures, however, the slope of the Arrhenius plot changes. Further experiments are being carried out to clarify the transport mechanisms and to shed light on the influence of Si NC on electrical transport.

## 5 CONCLUSION

Silicon nanocrystals in dielectric matrices such as SiC, $SiO_2$ or $SiN_x$ have promising features to be used as absorbers in all-Si tandem solar cells. The optical and electrical properties of SiC thin films incorporating silicon nanocrystals were studied. The band gap of the as-deposited films can be controlled by the composition of the film. The PL intensity of annealed films is strongly depended on annealing temperature and reaches a maximum after annealing at 950 °C. It is blueshifted 0.7 eV compared to the as-deposited sample. In-situ doping with diborane leads to enhanced conductivity of the SiC films. The effect of phosphorus doping could not be investigated unambiguously due to technological restrictions. The temperature dependence of the SiC films under investigation is in agreement with earlier results from other authors, but further experiments are necessary to clarify the role of Si nanocrystals in electrical transport.

## 6 ACKNOWLEDGMENTS

The authors thank Bernd Steinhauser, Janina Löffler, Anke Witzky and Rena Gradmann for measurements and discussion. This work was funded by the German Federal Ministry for the Environment, Nature Conservation and Nuclear Safety under contract number 0329849A “Th-ETA”. P. Löper gratefully acknowledges the scholarship support from the Reiner Lemoine Stiftung, and the ideational support from the Heinrich Böll Stiftung.

## 7 REFERENCES

[1] G. Conibeer, M. Green, E.-C. Cho, D. König, Y.-H. Cho, T. Fangsuwannarak, G. Scardera, E. Pink, Y. Huang, T. Puzzer, et al., Thin Solid Films 516 (2008) 6748.

[2] R. Rölver, B. Berghoff, D. Bätzner, B. Spangenberg, H. Kurz, M. Schmidt and B. Stegemann, Thin Solid Films 516 (2008) 6763.
[3] D. Song, E.-C. Cho, G. Conibeer, C. Flynn, Y. Huang and M.A. Green, Solar Energy Materials & Solar Cells 92 (2008) 474.
[4] X.J. Hao, E.-C. Cho, G. Scardera, Y.S. Shen, E. Bellet-Amalric, D. Bellet, G. Conibeer and M.A. Green, Solar Energy Materials & Solar Cells 93 (2009) 1524.
[5] M.A. Green, G. Conibeer, I. Perez-Wurfl, S.J. Huang, D. König, D. Song, A. Gentle, X.J. Hao, S.W. Park, F. Gao, et al., Proceedings of the 23rd European Photovoltaic Solar Energy Conference, Valencia, Spain (2008) 1.
[6] M. Zacharias, J. Heitmann, R. Scholz, U. Kahler, M. Schmidt and J. Bläsing, Applied Physics Letters 80 (2002) 661.
[7] M. Künle, in preparation (2009).
[8] F. Iori, E. Degoli, R. Magri, I. Marri, G. Cantele, D. Ninno, F. Trani, O. Pulci and S. Ossicini, Physical Review B 76 (2007) 085302/1.
[9] S. Ossicini, E. Degoli, F. Iori, O. Pulci, G. Cantele, R. Magri, O. Bisi, F. Trani and D. Ninno, Surface Science 601 (2007) 2724.
[10] R. Lechner, A.R. Stegner, R.N. Pereira, R. Dietmueller, M.S. Brandt, A. Ebbers, M. Trocha, H. Wiggers and M. Stutzmann, Journal of Applied Physics 104 (2008) 053701/1.
[11] A.R. Stegner, R.N. Pereira, K. Klein, R. Lechner, R. Dietmueller, M.S. Brandt, M. Stutzmann and H. Wiggers, Physical Review Letters 100 (2008) 026803/1.
[12] S. Park, B. Cho, X. Hao, G. Conibeer and M.A. Green, Proceedings of the 23rd European Photovoltaic Solar Energy Conference, Valencia, Spain (2008) 189.
[13] J. Tauc, R. Grigorovici and A. Vancu, physica status solidi (b) 15 (1966) 627.
[14] W. Siebert, R. Carius, W. Fuhs and K. Jahn, Physica Status Solidi B 140 (1987) 311.
[15] H.H. Berger, Journal of the Electrochemical Society 119 (1972) 507.
[16] R. Carius, K. Jahn, W. Siebert and W. Fuhs, Journal of Luminescence 31-32 (1984) 354.
[17] M. Vetter, C. Voz, R. Ferre, I. Martín, A. Orpella, J. Puigdollers, J. Andreu and R. Alcubilla, Thin Solid Films 511-512 (2006) 290.
[18] S. Janz. in Fakultät für Physik, pp. 227, Universität Konstanz, Freiburg im Breisgau 2006.
[19] D.A. Anderson and W.E. Spear, Philosophical Magazine 35 (1977) 1.
[20] J. Bullot and M.P. Schmidt, Physica Status Solidi B 143 (1987) 345.